LUNG VENTILATION

Preventing loss of mechanosensation by the nuclear membranes of alveolar cells reduces lung injury in mice during mechanical ventilation

Inés López-Alonso[1,2,3,4], Jorge Blázquez-Prieto[1,2,3,4], Laura Amado-Rodríguez[1,3,4], Adrián González-López[4,5], Aurora Astudillo[6,7], Manuel Sánchez[8], Covadonga Huidobro[1,3,4], Cecilia López-Martínez[2,3], Claudia C. dos Santos[9], Guillermo M. Albaiceta[1,2,3,4]*

The nuclear membrane acts as a mechanosensor that drives cellular responses following changes in the extracellular environment. Mechanically ventilated lungs are exposed to an abnormally high mechanical load that may result in clinically relevant alveolar damage. We report that mechanical ventilation in mice increased the expression of Lamin-A, a major determinant of nuclear membrane stiffness, in alveolar epithelial cells. Lamin-A expression increased and nuclear membrane compliance decreased in human bronchial epithelial cells after a mechanical stretch stimulus and in a murine model of lung injury after positive-pressure ventilation. Reducing Lamin-A maturation by depletion of the protease-encoding gene *Zmpste24* preserved alveolar nuclear membrane compliance after mechanical ventilation in mice. Ventilator-induced proapoptotic gene expression changes and lung injury were reduced in mice lacking *Zmpste24* compared to wild-type control animals. Similarly, treatment with the human immunodeficiency virus protease inhibitors lopinavir and ritonavir reduced the accumulation of Lamin-A at nuclear membranes and preserved nuclear membrane compliance after mechanical ventilation, mimicking the protective phenotype of *Zmpste24*$^{-/-}$ animals. These results show that the pathophysiological response to lung mechanical stretch is sensed by the nuclear membranes of lung alveolar cells, and suggest that protease inhibitors might be effective in preventing ventilator-induced lung injury.

INTRODUCTION

Mechanosensation of the environment is a major determinant of cell fate. By sensing the mechanical properties of its surroundings, cells activate or inhibit critical programs such as differentiation, proliferation, or programmed death (*1*). The major determinant of tissue stiffness is the extracellular matrix, which is physically connected to the cytoskeleton by transmembrane protein complexes (*2*). These elements converge in the nuclear membrane, which acts as the true cell mechanosensor (*3*). The stiffness of the nuclear membrane is determined, among others, by the amount of Lamin-A and Lamin-B in the nuclear lamina. An increase in Lamin-A/Lamin-B ratio in response to a rise in extracellular stiffness decreases nuclear compliance and regulates gene expression by modulating the organization of the underlying chromatin (*4*). However, Lamin-A is not the only factor, because mice lacking this specific isoform have a normal development (*5*).

Lung parenchyma is exposed to mechanical stress with each breath. Positive-pressure ventilation substantially increases lung stretch. In injured lungs, this can be further exacerbated by heterogeneous aeration, resulting in anisotropic inflation (*6*). Heterogeneous distribution of inspired gas may expose certain areas, such as air-liquid interfaces in damaged alveoli, to an increased mechanical load. The tissue response triggered by this stretch can activate inflammation and extracellular matrix remodeling, causing ventilator-induced lung injury (VILI) (*7*). Even in the absence of ultrastructural damage, mechanical forces can alter gene expression profiles promoting a proinflammatory response (*8*). Minimizing VILI has been shown to improve clinical outcomes in mechanically ventilated patients, especially in those with acute respiratory distress syndrome (ARDS) or at risk for VILI such as during major surgery (*9*, *10*). Treatments directed at preventing the response of the cell to mechanical stress might be an effective strategy to mitigate VILI.

Here, we postulated that blocking nuclear mechanosensation may represent a useful strategy to specifically target the pulmonary response to pathological stretch. To test this hypothesis, we studied nuclear dynamics in a variety of in vivo and in vitro models of lung stretch and in samples from ventilated and nonventilated patients to determine whether molecular manipulation of these mechanisms might prevent VILI.

[1]Área del Corazón, Hospital Universitario Central de Asturias, 33011 Oviedo, Spain. [2]Departamento de Biología Funcional, Instituto Universitario de Oncología del Principado de Asturias, Universidad de Oviedo, 33005 Oviedo, Spain. [3]Instituto de Investigación Sanitaria del Principado de Asturias, 33011 Oviedo, Spain. [4]Centro de Investigación Biomédica En Red–Enfermedades Respiratorias, Instituto de Salud Carlos III, 28029 Madrid, Spain. [5]Department of Anesthesiology and Operative Intensive Care Medicine, Charité Universitätsmedizin, 10117 Berlin, Germany. [6]Servicio de Anatomía Patológica, Hospital Universitario Central de Asturias, 33011 Oviedo, Spain. [7]Departamento de Cirugía y Especialidades Médicoquirúrgicas, Universidad de Oviedo, 33005 Oviedo, Spain. [8]Área de Farmacología, Departamento de Medicina, Universidad de Oviedo, 33005 Oviedo, Spain. [9]Interdepartmental Division of Critical Care, Keenan Research Centre of the Li Ka Shing Knowledge Institute of St. Michael's Hospital, University of Toronto, Toronto, Ontario M5B 1WB, Canada.
*Corresponding author. Email: guillermo.muniz@sespa.es

RESULTS

Changes in nuclear lamina after lung stretch

We first determined whether positive-pressure ventilation induced a change in the abundance of nuclear lamins. We measured lamin content in lung homogenates from mice ventilated with high (20 cmH_2O) or moderate (15 cmH_2O) driving pressure compared to normal ventilation. The abundance of Lamin-A in nuclear extracts was significantly increased in mice ventilated with high driving pressures ($P = 0.015$ for the effect of ventilation; Fig. 1A and fig. S1, A and B). The ratio of Lamin-A/Lamin-B, a major determinant of nuclear stiffness (*3*), was also increased after both moderate- and

high-pressure mechanical ventilation ($P = 0.002$ for the effect of ventilation; Fig. 1B). Increase in Lamin-A content was associated with a significant increment in both products of *Lmna* gene expression, coding for Lamin-A and Lamin-C ($P = 0.02$ for each one; Fig. 1C). The increased expression was also reflected in a stronger staining of Lamin-A in the nuclear lamina (Fig. 1D and fig. S1C). Similarly, lung tissue samples from critically ill patients (table S1) demonstrated a stronger LAMIN-A staining in the nuclear envelope in alveoli of those who received mechanical ventilation compared to nonventilated patients ($P = 0.018$ for the effect of ventilation), with no changes in LAMIN-B staining (Fig. 1, E and F). We did not detect a significant difference between patients with ARDS versus those without ARDS. Representative histological sections of airway epithelium and endothelium are shown in fig. S2 (A and B).

Next, we explored changes in nuclear stiffness by micropipette aspiration (Fig. 1G). We applied equibiaxial stretch for different times to human bronchial epithelial cells (BEAS-2b) and measured their lamin content and nuclear compliances. LAMIN-A/LAMIN-B ratio increased after 30 min of stretch, and this persisted up to 60 min ($P < 0.001$ in ANOVA; fig. S3, A and B). In separate experiments, cells were stretched for 1 hour and then left in static conditions for assessing recovery time. After 30 min of recovery, LAMIN-A/LAMIN-B ratio returned to baseline values (fig. S3B). In parallel, nuclear compliance significantly decreased with mechanical stretch ($P < 0.0001$ in ANOVA; Fig. 1H). During the recovery phase, compliance was still reduced after 10 min but returned to baseline values at 30 and 60 min (Fig. 1H). In contrast, when human lung fibroblasts (MRC-5 cell line) were subjected to the same mechanical stretch, no changes in LAMIN-A/LAMIN-B ratio or nuclear compliance were observed (fig. S3, C to E). These results suggest that stretch triggers a unique response within lung epithelial cells.

Changes in nuclear compliance and development of lung injury

To clarify the role of the nuclear envelope in VILI, we studied the effects of mechanical ventilation in $Lmna^{LCS/LCS}$ mice, which lack Lamin-A but have only minimal alterations in nuclear membrane dynamics (*5*). After mechanical ventilation, these mice showed a similar injury to their wild-type counterparts (fig. S4, A and B). Nuclear compliance decreased after ventilation (fig. S4C), and there were no differences in *Egr1* or *Ier3* gene expression, markers of mechanosensation(fig. S4, D and E). Therefore, absence of Lamin-A with preserved nuclear mechanics did not prevent lung injury after mechanical ventilation.

Then, we studied the effects of mechanical stretch in animals with more severe abnormalities of the nuclear envelope and its mechanical properties, such as the $Zmpste24^{-/-}$ mice. The protein encoded by this gene is a metallopeptidase involved in the processing of Lamin-A, so that loss of *Zmpste24* results in abnormal Lamin-A maturation and accumulation of Prelamin-A (*11*). Accumulation of Prelamin-A results in severe abnormalities of the nuclear envelope and accelerated aging (*12*). $Zmpste24^{-/-}$ mice exposed to mechanical ventilation with two different driving pressures are partially protected from VILI compared to wild type; $Zmpste24^{-/-}$ mice developed lower histological injury scores and decreased alveolocapillary permeability (Fig. 2, A to C). In line with these findings, mutant mice showed preserved oxygenation (Fig. 2D) and lung compliance (Fig. 2E) after ventilation with a pressure of 15 cmH_2O. Decreased susceptibility to injury as determined by decreased evidence of histological damage was likely not due to a differential inflammatory response, as the changes in lung neutrophilic infiltration (fig. S5, A and B), *Il6* (fig. S5C), or *Cxcl2* (fig. S5D) gene expression were similar in both genotypes.

As expected, absence of *Zmpste24* resulted in accumulation of Prelamin-A and no changes in protein concentration with ventilation (Fig. 2F and fig. S6A), but with an increase in Lamin-B only after ventilation with a peak pressure of 20 cmH_2O (fig. S6B). The Prelamin-A/Lamin-B ratio in these animals was not changed (Fig. 2G). Immunohistochemical studies confirmed the increase in mature Lamin-A in wild-type animals after mechanical ventilation and an accumulation of Prelamin-A in gene-deficient mice (fig. S7, A to C).

Next, we measured nuclear stiffness in nuclei isolated from mice lung tissue under baseline conditions and immediately after exposure to ventilation. After mechanical ventilation, nuclei from wild-type animals became stiffer compared to nuclei from $Zmpste24^{-/-}$ mice (Fig. 2H). Electron microscopy studies revealed a more euchromatic nucleus after mechanical ventilation in wild-type mice, but with persistence of heterochromatin foci in $Zmpste24^{-/-}$ mice (Fig. 2I). This difference correlated to a higher expression of mechanosensitive genes *Egr1* and *Ier3* in knockout mice after mechanical ventilation (Fig. 2, J and K). In addition, in vitro silencing of *ZMPSTE24*, but not *LMNA*, resulted in increased *EGR1* expression in human bronchial epithelial cells (BEAS-2b) exposed to equibiaxial cyclic stretch, reinforcing the validity of our in vivo results (Fig. 2L).

Finally, to determine whether the protective effect was restricted to mechanical ventilation, we studied $Zmpste24^{-/-}$ and wild-type mice after lipopolysaccharide (LPS) injection in lungs. There were no differences between genotypes in lung injury parameters or mechanosensitive gene expression (fig. S8, A to E).

Proapoptotic cell reprogramming after stretch

To characterize the biological mechanisms by which nuclear membrane stiffness alters susceptibility to lung injury, we profiled pulmonary gene expression in $Zmpste24^{-/-}$ mice under baseline conditions and after mechanical ventilation [microarray data available at Gene Expression Omnibus (GEO), accession number GSE85269]. Principal components analysis showed clustering of each sample according to ventilation and genotype (fig. S9). A total of 3050 genes were significantly changed by mechanical ventilation in both genotypes (with an adjusted *P* value lower than 0.05; Fig. 3A). Top 200 differentially expressed genes are shown in Fig. 3B. There was a predominance of up-regulated genes in $Zmpste24^{-/-}$ after ventilation compared to wild-type mice.

To test the hypothesis that the response to mechanical stress differs depending on the stiffness of the nuclear lamina (the different genotypes), we focused on 24 genes for which mechanosensitivity has been previously reported (*13*–*20*). Among these, a majority was overexpressed in ventilated $Zmpste24^{-/-}$ compared to wild-type mice (fig. S10, A and B).

Functional enrichment of differential transcriptomic profiles was performed using Ingenuity Pathway Analysis software to identify predicted functional differences between genotypes. This analysis showed that a number of pathways related to cell death, cell cycle arrest, and proliferation were differentially activated between wild-type and $Zmpste24^{-/-}$ mice after ventilation (Fig. 3C). In addition, differential expression of the 1855 genes annotated to "programmed cell death" category of the Gene Ontology database (AmiGo 2.0,

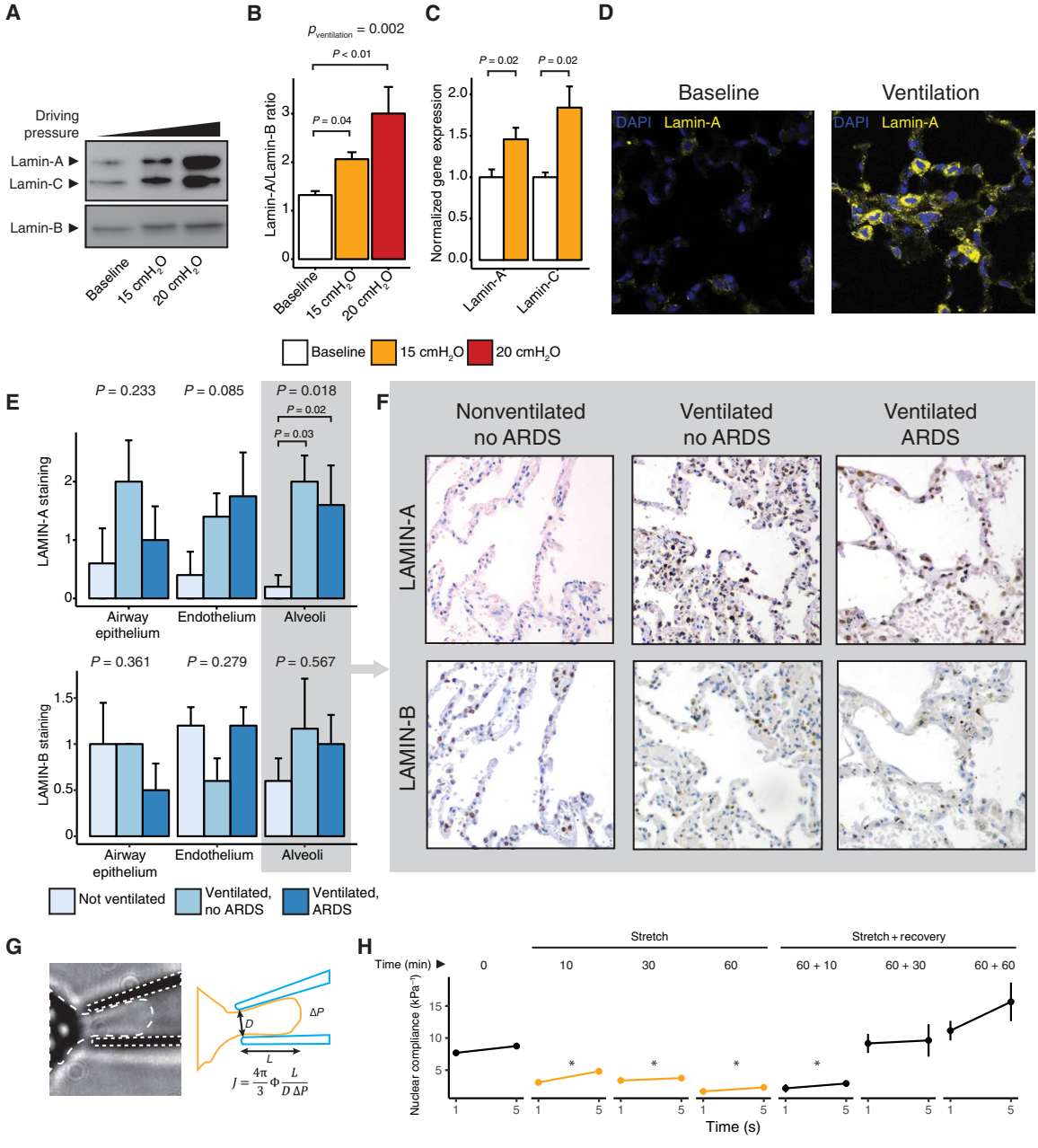

Fig. 1. Scaling of nuclear lamins with driving pressures in alveolar epithelium. (**A**) Representative Western blot showing Lamin-A, Lamin-B, and Lamin-C abundance during spontaneous breathing (baseline) or during mechanical ventilation with different driving pressures (15 and 20 cmH_2O) [means ± SEM, *P* value obtained using one-way analysis of variance (ANOVA); brackets indicate significant post hoc comparisons using a Tukey's honest significant difference (HSD) test; $n = 5$ per condition]. (**B** and **C**) Bar graph showing Lamin-A/Lamin-B ratio (B; $n = 5$ per condition) and *Lmna* gene expression (C; $n = 8$ per condition) at baseline and during mechanical ventilation. Data are shown as means ± SEM, *P* values obtained using a *t* test. (**D**) Representative immunofluorescence of lungs from spontaneous breathing (Baseline) and mechanically ventilated mice (with a driving pressure of 15 cmH_2O). DAPI, 4′,6-diamidino-2-phenylindole. (**E**) Bar graphs showing LAMIN-A (top) and LAMIN-B (bottom) expression in airway epithelium, endothelium, and alveoli in lung samples from autopsies of patients who died during spontaneous breathing ($n = 5$) or mechanical ventilation alone or in combination with ARDS ($n = 5$ and $n = 7$, respectively). Data are shown as means ± SEM; *P* values indicate comparison between ventilated and nonventilated patients using two-way ANOVA including lung injury and ventilation as factors, followed by Tukey's HSD post hoc test when significant (brackets). (**F**) Representative histology of alveoli showing LAMIN-A and LAMIN-B expression in patients described in (E). (**G**) Schematic representation of nuclear compliance measurements using micropipette aspiration. (**H**) Changes in compliance of nuclei (means ± SEM; $n = 3$ per group) from BEAS-2b cells at different times after stretch and recovery (*P* values obtained in the repeated-measurements ANOVA; asterisks represent a *P* value lower than 0.05 in Tukey's HSD post hoc tests when compared to baseline values).

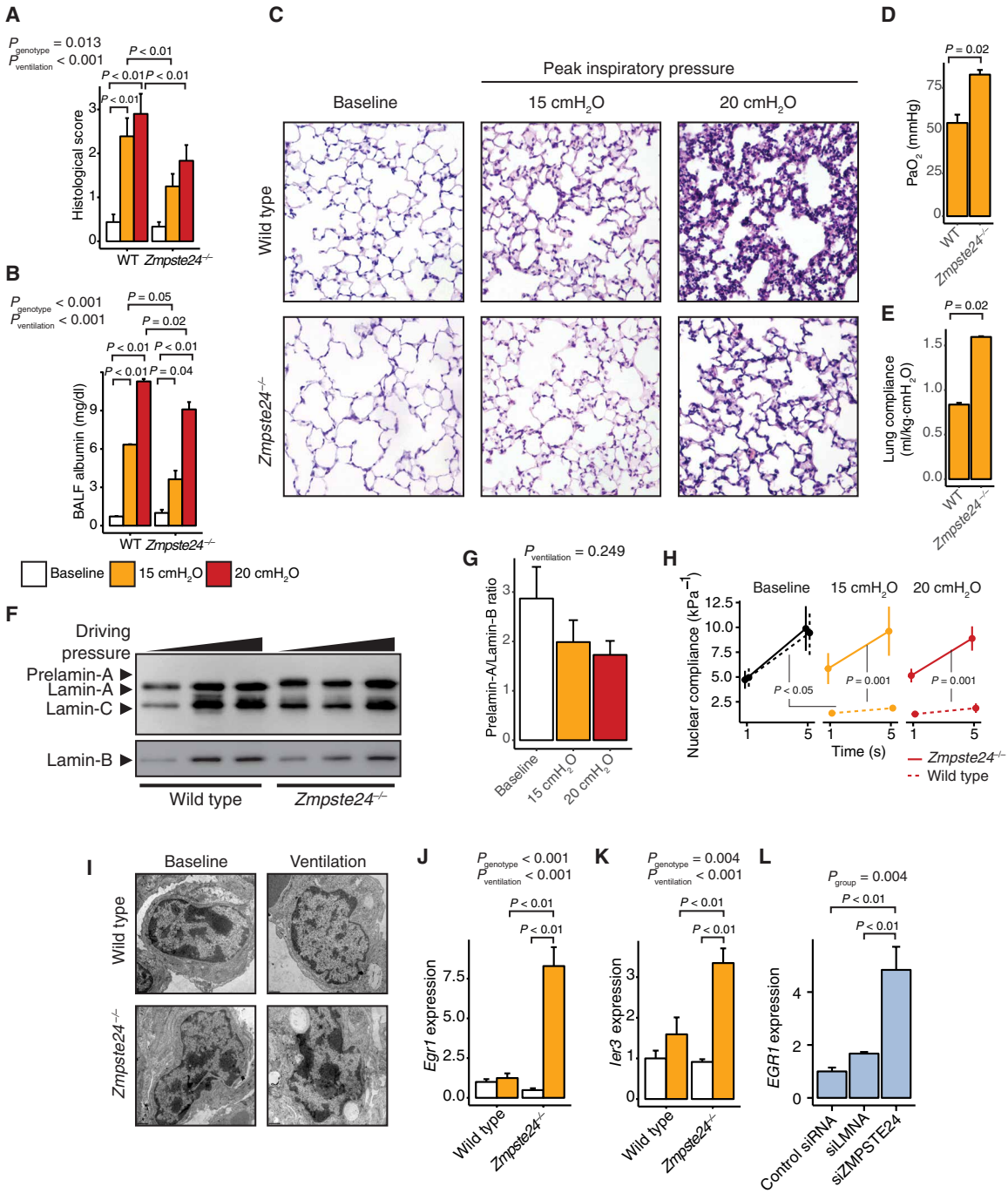

Fig. 2. Lung injury in *Zmpste24*-deficient mice. (**A** and **B**) Bar graphs showing lung damage after mechanical ventilation in wild-type and *Zmpste24*$^{-/-}$ mice, measured by a histological scale (A) or the albumin content of bronchoalveolar lavage fluid (BALF; B). *P* values obtained using two-way ANOVA including genotype and ventilation as factors; brackets indicate significant post hoc comparisons using a Tukey's HSD test; $n = 8$ per condition and genotype. (**C**) Representative histological lung sections. (**D** and **E**) Values of arterial PO_2 (D) and lung compliance (E) after ventilation with a driving pressure of 15 cmH_2O. *P* value obtained using a *t* test; $n = 4$ per genotype and condition. (**F**) Representative Western blot showing the presence of Prelamin-A in mutant mice compared to the mature form observed in wild-type animals. (**G**) Quantification of Prelamin-A/Lamin-B ratio in *Zmpste24*$^{-/-}$ mice in baseline conditions or after ventilation with 15 or 20 cmH_2O driving pressure ($n = 5$ per group; *P* value obtained using one-way ANOVA). (**H**) Graphs showing nuclear compliance measured by micropipette aspiration of nuclei from lungs of wild-type and *Zmpste24*$^{-/-}$ mice in baseline conditions and after mechanical ventilation ($n = 6$ per condition and genotype; *P* values obtained using one-way ANOVA; brackets show *P* values of Tukey's HSD post hoc comparisons). (**I**) Representative images of electron microscopy showing chromatin rearrangement in response to mechanical ventilation in nuclei from wild-type and mutant animals. (**J** and **K**) Expression of the mechanosensitive genes *Egr1* (H) and *Ier3* (I) [*P* values obtained using two-way ANOVA including genotype and ventilation as factors, followed by Tukey's HSD post hoc test when significant (brackets); $n = 8$ per condition and genotype]. (**L**) Effects of silencing *ZMPSTE24* or *LMNA* expression in human bronchial cells subjected to stretch compared to pretreatment with a sham small interfering RNA (siRNA) [*P* values obtained using one-way ANOVA, followed by Tukey's HSD post hoc test (brackets), are depicted in the graph; n=3 per group]. All data are shown as means ± SEM.

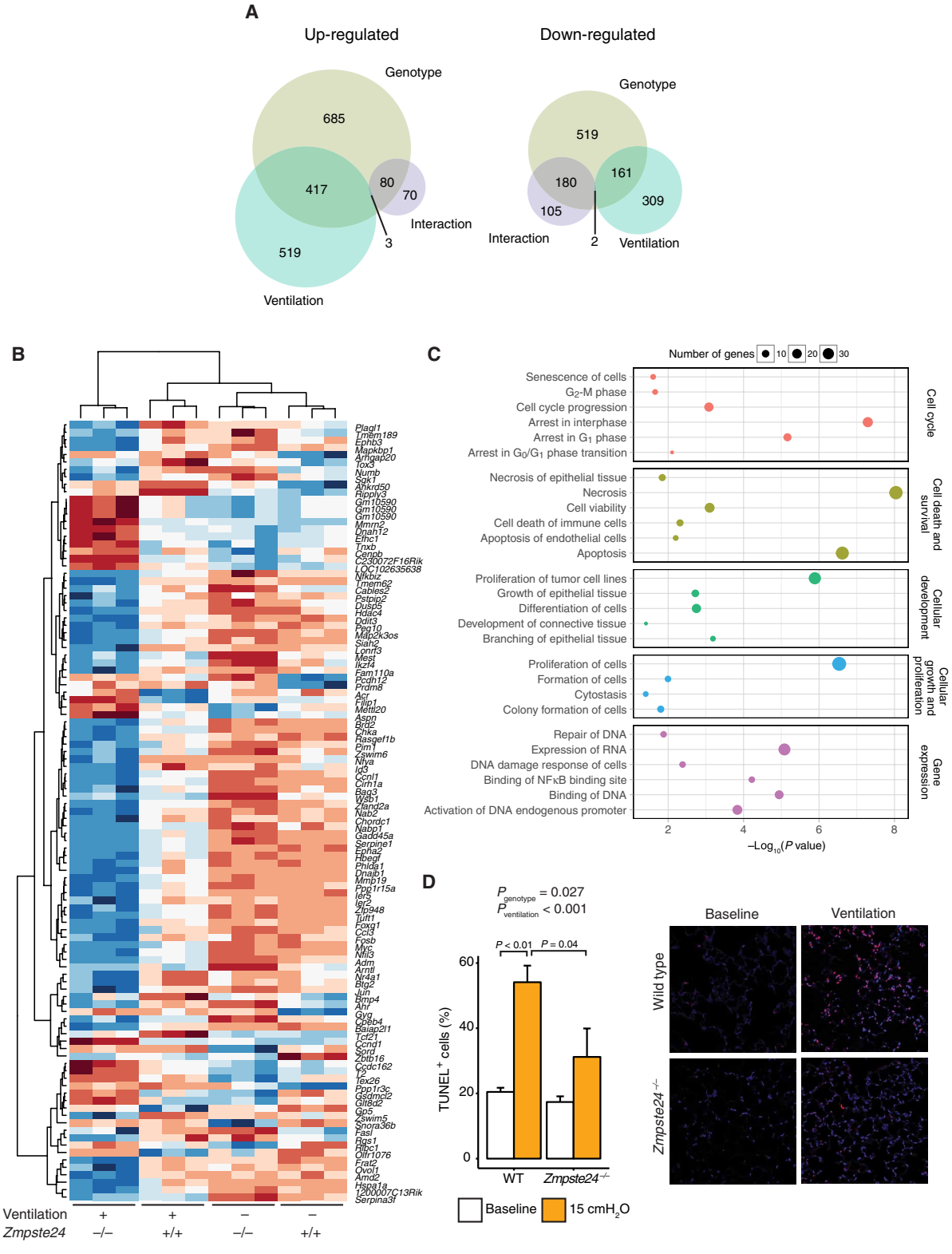

Fig. 3. Differential gene expression in lungs from *Zmpste24*$^{-/-}$ mice subjected to mechanical ventilation. (**A**) Venn's diagram showing the number of genes with significantly different expression after mechanical ventilation in wild type and *Zmpste24*$^{-/-}$ mice. (**B**) Heat map of the 200 genes with the top differential expression. (**C**) Graph showing the number of genes and the significance level of biological processes corresponding to the differentially expressed genes, according to the Ingenuity Pathway Analysis. NFκB, nuclear factor κB. (**D**) Bar graph showing the percentage of apoptotic cells in response to ventilation in wild-type and *Zmpste24*$^{-/-}$ mice. *P* values obtained using two-way ANOVA including genotype and ventilation as factors, followed by Tukey's HSD post hoc test when significant (brackets), and representative images of TUNEL staining. All data are shown as means ± SEM unless otherwise specified.

www.geneontology.org) was analyzed. Among these, there were 46 genes with differential response to ventilation (fig. S11, A and B).

The relative contribution of programmed cell death to the lung injury susceptibility phenotype was confirmed by TUNEL (terminal deoxynucleotidyl transferase–mediated deoxyuridine triphosphate nick end labeling) assays. The number of apoptotic cells ($TUNEL^+$) was increased in wild-type animals after ventilation, in line with previous findings (*21*). There were significantly lower apoptotic cells in $Zmpste24^{-/-}$ compared to wild-type mice ($P = 0.027$ for the effect of genotype; Fig. 3D). There were no differences between genotypes in apoptotic cell counts after LPS exposure, confirming the mechanosensitive nature of this response (fig. S12, A and B).

Effects of HIV protease inhibitors on nuclear compliance and lung injury

Finally, we used pharmacological manipulation to alter nuclear dynamics and determine the conceptual feasibility of this approach as a therapeutic strategy for VILI. HIV protease inhibitors lopinavir/ritonavir may inhibit ZMPSTE24 (*22*). We randomized wild-type mice to intraperitoneal lopinavir/ritonavir or placebo treatment for 5 days. Lopinavir/ritonavir- and placebo-treated mice were further randomized to positive-pressure ventilation or spontaneous breathing. In terms of treatment effectiveness, we could not demonstrate Zmpste24 inhibition because Prelamin-A was not detected in Western blots of nuclear extracts after 5 days of treatment (Fig. 4A); however, we were able to document a significant decrease in Lamin-A/Lamin-B ratios in treated mice after positive-pressure ventilation ($P = 0.003$ for the effect of treatment in two-way ANOVA; Fig. 4B). The distribution of Lamin-A was different in lopinavir/ritonavir- versus placebo-treated mice. In vehicle-treated mice, Lamin-A staining was almost limited to the nuclear lamina, whereas in those animals treated with lopinavir/ritonavir, the protein was spread along the nucleoplasm and, to a lesser extent, the cytoplasm (Fig. 4C).

The functional consequences of the treatment were an absence of nuclear stiffening after ventilation (Fig. 4D) and an increase in the expression of the mechanosensitive gene *Egr1* (Fig. 4E), resembling the results previously obtained in $Zmpste24^{-/-}$ animals. As hypothesized, mice treated with lopinavir/ritonavir developed only mild lung injury after ventilation compared to those that received vehicle alone (Fig. 4F), with preservation of alveolocapillary permeability (Fig. 4G), oxygenation (Fig. 4H), and lung compliance (Fig. 4I). In addition, the number of apoptotic cells in lopinavir/ritonavir-treated mice was also decreased (Fig. 4J).

Treatment with lopinavir/ritonavir did not show any benefit on lung damage or epithelial apoptosis (fig. S13, A and B), nor increased lung *Egr1* expression in $Lmna^{LCS/LCS}$ mice (fig. S13C), suggesting again that the benefits of the therapy in wild-type animals are related to the preservation of the nuclear compliance driven by an abnormal distribution of Lamin-A. Similarly, treatment of $Zmpste24^{-/-}$ mice with these drugs did not lead to further improvements in lung injury (fig. S14, A to C).

To further confirm the specificity of this treatment for stretch-induced injury and to assess its safety, wild-type mice were ventilated to induce moderate injury (peak pressure, 15 cmH_2O), extubated, and left to recover on spontaneous breathing for 48 hours. Immediately after extubation, mice were randomized to receive lopinavir/ritonavir or vehicle. After 48 hours, the lung injury improved with no differences between groups (fig. S15A). Lamin-A/Lamin-B ratios were similar between groups (fig. S15B). However, treated animals showed differences in expression of p53-dependent genes such as *p21* or *Gadd45a* (fig. S15, C and D, respectively).

Collectively, these results suggest that interference with the physiological nuclear stiffening induced by lung stretch may be a specific therapeutic strategy to avoid VILI, although this treatment could have long-term adverse effects derived from the activation of the p53 pathway.

DISCUSSION

The results presented in this study provide evidence that mechanical ventilation modifies the mechanical properties of the nuclear envelope. Using both an animal model of VILI and samples from patients, we show that mechanical ventilation alters the stiffness of the nuclear membrane of alveolar epithelial cells. Moreover, our data suggest that this change has pathophysiological implications, because its manipulation ameliorates the lung damage caused by mechanical stretch in rodents.

Mechanotransduction has emerged as a key mechanism that guides the cell fate (*23*). There is a large variety of cell structures that may act as mechanosensors. The plasma membrane has force-sensing ion channels (*24*), and the cytoskeleton can trigger intracellular signaling cascades (*25*). Moreover, the cytoskeleton may transmit the forces from the extracellular matrix to different organelles such as mitochondria or the nucleus. All these structures have been involved in mechanosensation by generation of cytoplasmic second messengers or rearrangement of the cytoskeleton itself in response to stretch. Although our work focused on nuclear mechanosensation, we cannot discard that targeting other structures could also avoid the transmission of forces and avoid the stretch-induced injury. Similarly, our results do not exclude that other cell populations such as fibroblasts could contribute to the lung response to stretch. Although under our experimental conditions there were no changes in the nuclear compliance of fibroblasts, different patterns of mechanical stretch may alter nuclear dynamics (*26*).

The nuclear membrane has been identified as one of the key cell mechanosensing structures that, in response to the extracellular stiffness, decreases its compliance (*3*). This change in stiffness occurs early after mechanical stretch, can be reverted, in line with previous findings (*27*), and results in a reduction in the expression of cyclic stretch–dependent genes. From a biological perspective, it is not surprising that mechanical deformation should have such a profound effect on cell biology. Cell lineage differentiation in response to the mechanical properties of the underlying substrate is one of the most paradigmatic examples of this phenomenon (*28*). However, this mechanism may also play a pathogenetic role in several diseases.

We postulate that once the mechanotransduction response to cellular deformation is triggered, intracellular signaling pathways converge in a relatively small number of cell responses, including inflammation or cell growth and survival. Lung epithelial apoptosis triggered by mechanical stretch has long been known to contribute to more severe injury (*29*). Expression of the mechanosensitive gene *Egr1* may trigger apoptosis itself (*30*). However, $Zmpste24^{-/-}$ mice had an anti-apoptotic phenotype as shown by the microarray data and subsequent pathway analysis, with increased expression of inhibitors of programmed cell death in respiratory cells, such as *Adm* (*31*), *Nr4a1* (*32*), *Pim1* (*33*), or *Cdkn1a* (*34*). Therefore, although *Egr1* is a marker of stretch-triggered gene expression, it is likely not

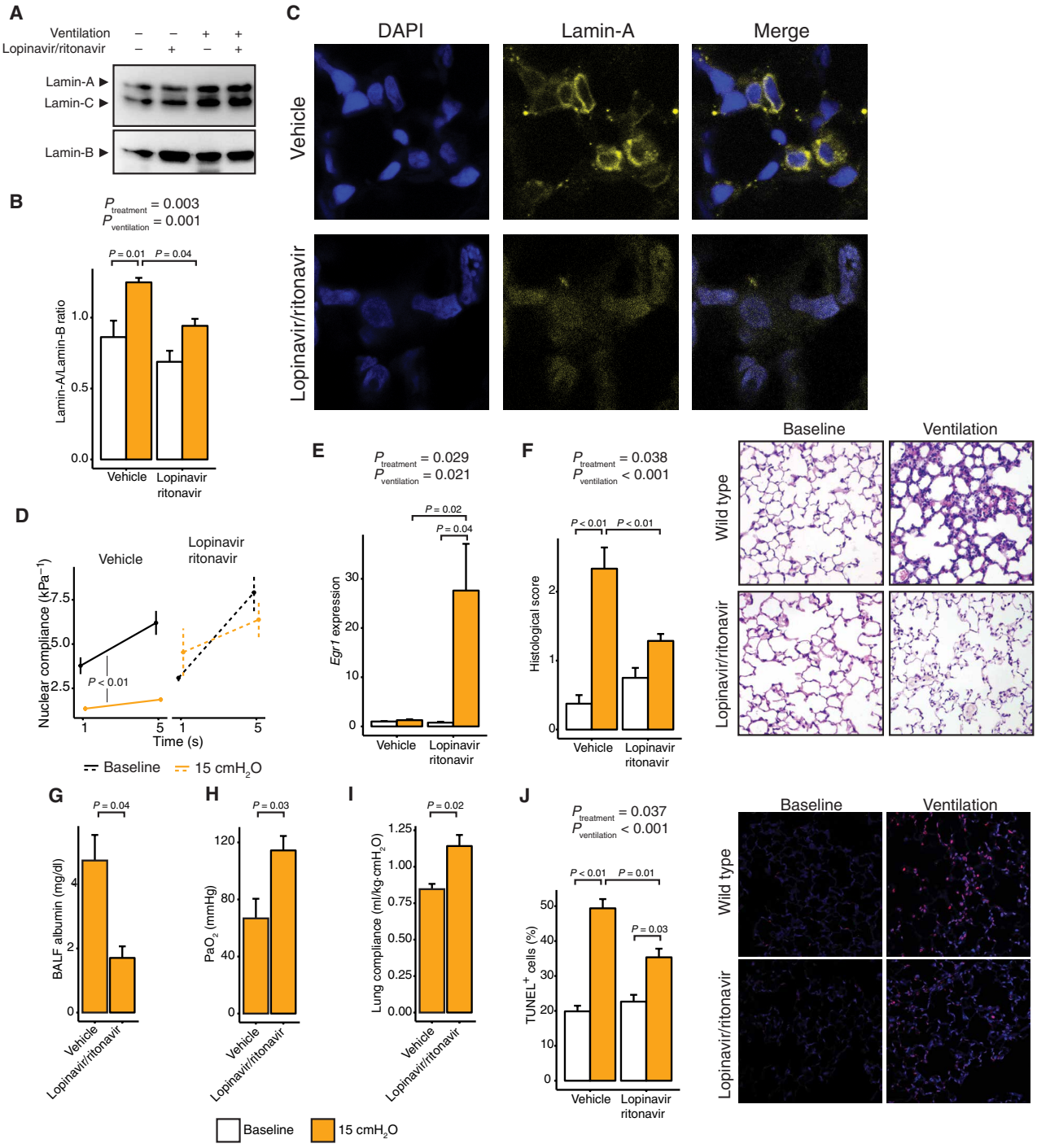

Fig. 4. Effects of lopinavir/ritonavir in VILI and nuclear compliance. (**A**) Representative Western blot of nuclear lamins in vehicle- and lopinavir/ritonavir-treated animals subjected to mechanical ventilation. (**B**) Bar graph showing changes in Lamin-A/Lamin-B ratio with treatment. *P* values obtained using two-way ANOVA including treatment and ventilation as factors, followed by Tukey's HSD post hoc test when significant (brackets); $n = 4$ per condition and treatment. (**C**) Immunofluorescence images illustrating the organization of nuclear Lamin-A after an intraperitoneal injection of lopinavir/ritonavir or its vehicle. (**D**) Nuclear compliance after mechanical ventilation in vehicle- and lopinavir/ritonavir-treated animals ($P = 0.003$ for the effect of treatment obtained using a repeated-measurements ANOVA, including ventilation, treatment, and time as factors, followed by Tukey's HSD test, depicted in the graph; $n = 4$ per condition and treatment). (**E**) Effects of treatment on *Egr1* gene expression. *P* values obtained using two-way ANOVA including treatment and ventilation as factors, followed by Tukey's HSD post hoc test when significant (brackets); $n = 4$ per condition and treatment. (**F** to **I**) Quantification of lung damage after ventilation in animals treated with vehicle or lopinavir/ritonavir using a histological score (F; $n = 8$ per condition and treatment; panels show representative sections stained with hematoxylin and eosin), albumin concentration in bronchoalveolar lavage fluid (G; $n = 5$ per group), PaO_2 (H; $n = 4$ per group), and lung compliance at the end of ventilation (I; $n = 4$ per group). *P* values obtained using *t* tests. (**J**) Apoptotic cell count after ventilation in vehicle- and lopinavir/ritonavir-treated mice ($n = 3$ per condition and treatment) and representative TUNEL staining in each experimental group. *P* values obtained using two-way ANOVA including treatment and ventilation as factors, followed by Tukey's HSD post hoc test when significant (brackets). All data are shown as means ± SEM.

responsible for the beneficial effects of targeting Zmpste24 to prevent VILI.

The relative unspecificity of the responses triggered by pathological mechanical stimuli makes it difficult to identify suitable therapeutic targets. Manipulation of convergent final pathways is often complicated by adverse "off-target" effects and fails to improve clinically relevant outcomes (*35*). In contrast, blockade of the mechanosensitive properties of the nuclear membrane may provide a specific proximal target that, by avoiding interference with core homeostatic processes such as the inflammatory response, may represent not only a plausible target for the prevention and treatment of VILI but also a strategy to promote repair (*36*). Genetic targeting using *Zmpste24* knockout mice confirms that preservation of nuclear elasticity specifically ameliorates lung damage caused by stretch. Despite the fragility observed in the adult mutant mice, *Zmpste24*$^{-/-}$ mice were significantly resistant to VILI but not to LPS injection, confirming the mechanical specificity of this response. Similarly, the isolated Lamin-A deletion yielded no differences in susceptibility to mechanical lung damage. The absence of benefits in *Lmna*$^{LCS/LCS}$ mice subjected to our model of lung injury points to the role of nuclear mechanics as the critical determinant of severity of injury, because they show no differences in nuclear compliances compared to wild-type animals. It has been described that Lamin-A is dispensable for the preservation of the nuclear structure (*5*). Moreover, in *LMNA*-deficient cells, the expression of mechanosensitive genes is decreased and apoptosis increased (*26*). These results resemble the rescue of the progeroid phenotype in *Zmpste24*$^{-/-}$ mice with *Lmna* heterozygosity (*12*) and suggest an active role of Prelamin-A.

These results strongly suggest that the blockade of mechanotransduction at the nuclear membrane might block the pathogenetic response to stretch. It has been shown that HIV protease inhibitors lopinavir/ritonavir can directly inhibit ZMPSTE24 (*22*). However, we and others have failed to demonstrate this effect in vivo (*37*). Our microscopy data show that treatment with lopinavir/ritonavir impairs the nuclear lamina assembling, keeping diffuse Lamin-A monomers or oligomers in the nucleoplasm, suggesting a possible defect in posttranslation protein regulation affecting localization. We cannot discard that other steps in Lamin-A processing, such as degradation, are also affected by this treatment. The impaired Lamin-A scaffolding blocks the physiological increase in nuclear stiffness observed in untreated animals, thus avoiding the cell reprogramming and development of a proapoptotic phenotype, ameliorating stretch-induced lung injury. Although HIV protease inhibitors have shown anti-apoptotic effects by direct caspase inhibition or by cell cycle arrest (*38*), our results link their beneficial effect to the preservation of nuclear mechanics and mechanosensitive gene expression. Moreover, lopinavir/ritonavir treatment was not effective in *Zmpste24*$^{-/-}$ or *Lmna*$^{LCS/LCS}$ mice, and the treatment did not show any benefit during the repair phase, once the injurious ventilation has been stopped and nuclear compliance restored.

Collectively, our findings support the idea that nuclear membrane compliance, and not Lamin-A itself, is the key mechanosensor. An active manipulation aimed to preserve this nuclear compliance may be helpful to avoid stretch-induced lung injury. In wild-type animals, the increase in nuclear stiffness dampens mechanosensitive gene expression, leading to apoptosis in alveolar cells (fig. S16A). Manipulating the stiffness of the nuclear membrane, either genetically (fig. S16B) or pharmacologically (fig. S16C), mitigates lung damage. These changes could be equivalent to a switch to a Lamin-B–dominant phenotype, with increased nuclear compliance and resistance to cell death (*39*), so different therapeutic approaches targeting other components of the nuclear envelope, such as Lamin-B, might yield similar results.

Our work has limitations that warrant some discussion. The animal model may not be fully representative of the characteristics of ventilator-associated lung injury in patients, and there may be other unidentified mechanisms in *Zmpste24*$^{-/-}$ animals that account for the results. However, the model has been widely used (*40*), and the significance and specificity of the findings have been confirmed by the occurrence of similar molecular mechanisms in human samples and the combination of a genome-wide search using microarrays with confirmatory experiments using other mutant animals or injury models. Another limitation comes from the risks related to long-term treatment with protease inhibitors. Animals treated for 5 days showed an increased expression of p53-dependent genes, thus raising concerns on their safety, in line with previously published reports.

In conclusion, our results suggest that the changes in nuclear membrane of pneumocytes act as a mechanosensor during lung stretch, promoting lung injury by increasing apoptosis. These results provide evidence that the nuclear membrane and its stiffness and composition are not only responsive to changes in the cell environment but might also represent a valid therapeutic target.

METHODS

Study design

The work was designed to study the role of the nuclear envelope in the lung response to mechanical stretch. *Zmpste24*$^{-/-}$ mice, *Lmna*$^{LCS/LCS}$ mice, and their wild-type counterparts were mechanically ventilated to induced different degrees of stretch-induced lung injury. The severity of lung damage and the responsible mechanisms were studied in tissues harvested from these animals, comparing different genotypes. In addition, mechanical properties of nuclei isolated after mechanical stretch were assessed by micropipette aspiration. All the measurements were performed blinded to the experimental conditions. Confirmatory experiments were performed in autopsy samples from patients who received mechanical ventilation and in cells cultured under equibiaxial stretch. In separate experiments, mice were treated with intraperitoneal LPS to induce lung inflammation without mechanical stretch. Finally, to mimic the beneficial results observed in *Zmpste24*$^{-/-}$ animals, wild-type mice were randomized to receive a prophylactic treatment with lopinavir/ritonavir before ventilation, to interfere with Lamin-A maturation, or vehicle. In these treated animals, lung injury, nuclear compliance, and apoptosis were studied. At least three biological replicates in culture experiments or five animals per group were used in all the experiments. Data were analyzed using *t* tests or one-way or two-way ANOVA according to the experimental design, with an $\alpha < 0.05$. Statistical power was calculated for the nonsignificant comparisons. All the animal experiments were performed according to the Animal Research: Reporting of In Vivo Experiments (ARRIVE) guidelines (*41*). Raw data were provided as a separate excel file (table S3).

Animal study

All experiments were approved and performed according to guidelines set out by the ethical committee for Animal Experimentation of the University of Oviedo, Spain. All animals were maintained in

specific pathogen–free conditions with 12-hour light and 12-hour dark cycles and ad libitum access to water and food. *Zmpste24*$^{-/-}$ mice (in pure C57Bl/6 background), *Lmna*$^{LCS/LCS}$ mice (in mixed C57Bl/6-129Sv background), and their respective wild-type counterparts were generated and genotyped as described (*5*, *11*).

Experimental models and tissue collection

Mice were anesthetized by intraperitoneal injection of a mixture of ketamine and xylazin. Then, a tracheostomy was performed, and the animals were connected to a mechanical ventilator (Evita 2 Dura-Neoflow, Drager). Mice of all genotypes were studied at baseline or after 2.5 hours of mechanical ventilation using two different levels of driving pressure to induce moderate or severe lung damage (15 cmH_2O, 100 breaths/min or 20 cmH_2O, 50 breaths/min, respectively)(*42*). Because wild-type and *Zmpste24*$^{-/-}$ mice showed no differences in respiratory , chest wall, or lung compliances at baseline conditions (fig. S17, A to C, respectively), equal driving pressures will yield equal tidal volumes.

Other ventilator settings were kept constant (zero end-expiratory pressure, inspiratory/expiratory ratio 1:1, and inspired oxygen fraction 0.21). Arterial blood samples were drawn from direct aortic puncture at the end of ventilation, and oxygen partial pressure was measured in a gasometer (Radiometer ABL90). Lung compliance was calculated with an open chest after injection of 1 ml of air, using a water column to measure pressure, and expressed as milliliter per kilogram of body weight and cmH_2O. In separate confirmatory experiments, *Lmna*$^{LCS/LCS}$ mice and their wild-type littermates were studied in baseline conditions or after moderate VILI.

In addition, *Zmpste24*$^{+/+}$ and *Zmpste24*$^{-/-}$ animals were intraperitoneally injected with LPS (20 mg/kg; serotype O55:B5, Sigma-Aldrich). After 8 hours, mice were anesthetized with ketamine/xylazin, and lungs were removed for biochemical assays and histological studies.

After the study period, animals were sacrificed by exsanguination, and the lungs were removed. The right bronchus was tied, and the right lung was frozen at −80°C for subsequent analysis. The left lung was fixed with intratracheal 4% formaldehyde and immersed in the same fixative for histological analysis. Additional animals, after either spontaneous breathing or mechanical ventilation, were used to perform a bronchoalveolar lavage. The albumin content in the recovered fluid was determined using the bromocresol green technique (*43*), and the absorbance was measured at 629 nm to assess the alveolocapillar permeability.

Lopinavir/ritonavir therapy

Wild-type, *Zmpste24*$^{-/-}$, and *Lmna*$^{LCS/LCS}$ mice were treated with lopinavir/ritonavir (100/25 mg/kg, intraperitoneally injected) or vehicle [10% ethanol in phosphate-buffered saline (PBS)] each 12 hours for 5 days. Then, the animals were randomized to spontaneous breathing or the same ventilation protocol as described above (peak inspiratory pressure, 15 cmH_2O). Finally, animals were sacrificed, and lungs were removed.

In addition, wild-type animals were ventilated (peak inspiratory pressure, 15 cmH_2O) for 2.5 hours to induce moderate lung injury. After ventilation, mice were treated with atropine (0.05 mg/kg), disconnected from the ventilator until awakening, and then extubated and left to recover under a heating lamp. Immediately after ventilation, mice were randomized to receive lopinavir/ritonavir (100/25 mg/kg each 12 hours, intraperitoneally injected) or vehicle and followed for 48 hours. After this period, mice were sacrificed and tissues were sampled as described.

Patients

Human lung samples were collected from the tissue bank at the Hospital Universitario Central de Asturias for immunohistochemistry analyses. Tissue samples were taken from lower lobes. Non-ventilated and ventilated patients with and without the ARDS (*44*) were selected for these analyses. Antibodies against LAMIN-A/C and LAMIN-B were used as described below.

Histological and immunohistochemical studies

After fixation, the left lung was embedded in paraffin, and three slices, with a minimal separation of 1 mm between them, were stained with hematoxylin and eosin. The severity and extent of lung injury after mechanical ventilation or LPS injection were evaluated by a pathologist blinded to the experimental conditions using a previously defined score (*43*).

For immunohistochemistry analyses, slides were deparaffinizated in xylene, boiled for 20 min in 0.1 M citrate buffer (pH 6.0) for antigen retrieval, and permeabilizated in 0.1% Triton X-100 in PBS for 15 min. Goat serum (10% in PBS) was used for blocking. Antibodies against Lamin-A/C (sc-20681, Santa Cruz Biotechnology) and Lamin-B (Cell Signaling Technology) were used, and the intensity of the staining was quantified from 0 to 4 by a pathologist blinded to experimental conditions. Cells were classified as epithelial, endothelial, or pneumocytes based on their morphology and histological location.

Neutrophilic infiltration within lung tissue was detected by immunohistochemistry using an antibody against myeloperoxidase (Thermo Fisher Scientific). The number of myeloperoxidase-positive cells was counted in three random fields (200×) and averaged.

Apoptotic cells in lung sections were detected by TUNEL. The number of apoptotic nuclei was counted in three random fields (400×) acquired in a Leica SP8 confocal microscope and expressed as percentage of the total nuclei count.

Electron microscopy

Mice were sacrificed by exsanguination, and the lungs were removed and fixed using a specific buffer with 3% glutaraldehyde and osmium tetroxide. Semithin sections were stained with toluidine blue to select regions of interest. Then, ultrathin sections (20 nm) were collected and stained with uranyl acetate and lead citrate. Images were taken using a JEOL 1011 transmission electron microscope.

Nuclear isolation

Fresh lung tissue was chopped using a blade, suspended in a buffer containing 1 M tris-HCl (pH 8), 0.5 M $MgCl_2$, 1 M KCl, 1 M dithiothreitol (DTT), and complete protease inhibitor cocktail (Roche), and homogenized using a Potter homogenizer. The resulting material was left in ice for 15 min and centrifuged at 850*g* for 10 min. After centrifugation, the pellet with the nuclei was resuspended in a nuclear isosmotic buffer [150 mM KCl, 4.198 mM $CaCl_2$, 5 mM EGTA, and 10 mM Hepes (pH 7.2)].

Nuclear mechanics

Freshly isolated nuclei were placed in an experimental chamber containing a buffer solution [150 mM KCl, 4.198 mM $CaCl_2$, 5 mM EGTA, and 10 mM Hepes (pH 7.2), giving 1 μM Ca^{2+}] and observed

via an inverted microscope (Nikon Diaphot 200). Buffer solution was continuously applied to the chamber (0.2 to 0.3 ml) by gravity at about 1 ml/min. Micropipettes were created from borosilicate glass tubes (Drummond Scientific) by means of a puller (L/M-3P-A, List Medical Electronic) and a microforge (MF-900, NARISHIGE) to create a flat tip. The micropipette tip was filled with the buffer solution and mounted in a micromanipulator connected to a digital pressure transducer, calibrated against a water column, and a syringe, using a three-way stopcock. Signals from the pressure transducer were recorded in a bedside monitor.

Using the micromanipulator, the pipette tip was placed on the nuclear membrane, and negative pressure was applied with the syringe. The deformation of the nucleus into the pipette tip was recorded using a charge-coupled device camera coupled to the microscope. The nuclear compliance was calculated from the aspirated length (L) and the pipette diameter (D) obtained in images captured 1 and 5 s after aspiration, the pressure applied (ΔP), and a geometry-dependent factor ($\Phi = 2.1$) according to Swift *et al.* (*3*). The applied formula reflects the ratio between the nuclear strain (defined as the quotient between the length of the nuclear extrusion and the pipette diameter) and the applied pressure (*45*). All the measurements obtained from the digital images were performed using the ImageJ software [National Institutes of Health (NIH)].

Cell stretch experiments

Human bronchial epithelial cells (BEAS-2b) or lung fibroblasts (MRC-5) were seeded onto BioFlex plates (Flexcell International) at a density of 3×10^5 cells per well and cultured for 48 hours until 80% confluence. Mycoplasma contamination was excluded in all the cultures. Mechanical stretch was performed for different times using a cell stretcher device in cell culture conditions (37°C, 21% O_2, 5% CO_2). In some experiments, cells were stretched for 60 min and then left in static conditions for different periods of time to address recover. Stretching rate was set at 15 cycles/min with a 1:1 stretch/relaxation ratio and a 18% maximal equibiaxial elongation. At the end of the experiments, cells were immediately processed and their proteins and RNA were extracted. In additional experiments, cells were then transfected with siRNA against *ZMPSTE24*, *LMNA*, or a control siRNA for 24 hours using Lipofectamine RNAiMAX, following the manufacturer's instructions.

Quantitative polymerase chain reaction

RNA was isolated from lung tissue samples or cells after homogenization with TRIzol (Sigma-Aldrich) and precipitated by adding isopropanol. After centrifugation and washing with ethanol, the pellet containing the RNA was resuspended in water. Complementary DNA (cDNA) was synthesized from 1 μg of total RNA using a standard RT-PCR kit (High-Capacity cDNA rtKit, Applied Biosystems). Quantitative polymerase chain reaction (qPCR) was carried out in triplicate for each sample using 40 ng of cDNA. SYBR PowerUp qPCR Master Mix (Applied Biosystems) and 10 μM of the specific primers were used for the genes encoding macrophage inflammatory protein-2 [*Cxcl2*, 5′-ATCCAGAGCTTGAGTGTGACG-3′ (forward) and 5′-GTTAGCCTTGCCTTTGTTCAG-3′ (reverse)], interleukin-6 [*Il6*, 5′-ACCACTTCACAAGTCGGAGG-3′ (forward) and 5′-TGCAAGTGCATCATCGTTGT-3′ (reverse)], lamin-A [*Lmna*, 5′-GGTTGAGGACAATGAGGATGA-3′ (forward) and 5′-TGAGCGCAGGTTGTACTCAG-3′ (reverse)], lamin-C [*Lmna*, 5′-GACAATGAGGATGACGACGAG-3′ (forward) and 5′-TTAATGAAAAGACTTTGGCATGG-3′ (reverse)], IEX-1 [*Ier3*, 5′-GAGCGGGCCGTGGTGTC-3′ (forward) and 5′-CTTGGCAATGTTGGGTTCCTC-3′ (reverse)], early growth response 1 [*Egr1*, 5′-CCTATGAGCACCTGACCACA-3′ (forward) and 5′-TCGTTTGGCTGGGATAACTC-3′ (reverse)], p21 [*cdkn1a*, 5′-GGAAACATCTCAGGGCCGAAA-3′ (forward) and 5′-AAGACCAATCTGCGCTTGGA-3′ (reverse)], gadd45a [*Gadd45a*, 5′-TGGAGGAAGTGCTCAGCAAG-3′ (forward) and 5′-GGGTCTACGTTGAGCAGCTT-3′ (reverse)], and glyceraldehyde-3-phosphate dehydrogenase as endogenous control [*Gadph*, 5′-GTGCAGTGCCAGCCTCGTCC-3′ (forward) and 5′-GCCACTGCAAATGGCAGCCC-3' (reverse)] (all from Sigma-Aldrich). The relative expression of the analyzed genes was calculated as $2^{\Delta Ct(\text{gene of interest})-\Delta Ct(Gadph)}$ and normalized to baseline conditions.

Microarray analysis

RNA was extracted from lung tissue using the RNeasy Kit (QIAGEN), and their quality was evaluated by capillary electrophoresis (Agilent 2100 Bioanalyzer). Affymetrix Mouse Gene 2.0 ST arrays were hybridized and scanned following the manufacturer's instructions. Raw values were processed (background correction and normalization) using the Robust Multichip Average Algorithm to obtain gene expression values. A principal components analysis was performed to characterize the overall differences in gene expression among groups.

Differences in gene expression among genotypes and ventilatory strategies were calculated by fitting expression to a linear model and computing the corresponding F statistics with Bayesian moderation of the standard errors. P values were adjusted using the Benjamini and Hochberg method. All the microarray analyses were performed with the limma and oligo packages for the statistical software R (R foundation for statistical computing). Data were additionally analyzed using the Ingenuity Pathway Analysis software to identify significant differences in mapped molecular and cellular functions.

Western blotting

Nuclei were homogenized in 50 mM tris (pH 7.4), 150 mM NaCl, 1% NP-40, 50 mM NaF, 1 mM DTT, and complete protease inhibitor cocktail (2 mg/ml; Roche). The whole amount of protein from homogenates was quantified using a BCA Protein Assay Kit (Pierce), and 15 μg from each sample was loaded in SDS-polyacrylamide gels. After electrophoresis at 120 mV, gels were electrotransferred onto polyvinylidene fluoride membranes, blocked with 3% nonfat dry milk, and incubated overnight at 4°C with 1:2000 anti–Lamin-A/C (sc-20681, Santa Cruz Biotechnology), 1:1000 anti–Lamin-B1 (sc-374015, Santa Cruz Biotechnology), and 1:10,000 anti-actin (sc-1616, Santa Cruz Biotechnology) in tris-buffered saline with 0.05% Tween 20. Finally, blots were incubated with 1:10,000 goat anti-rabbit horseradish peroxidase (HRP; sc-2004, Santa Cruz Biotechnology) or 1:10,000 anti-mouse HRP (sc-2005, Santa Cruz Biotechnology) in 1.5% nonfat milk. Proteins were detected by chemiluminescence in a ChemiDoc camera (UVP), and the intensity of each band was quantified in digital images using the ImageJ software (NIH).

Statistical analysis

Results are expressed as means ± SEM. Data were analyzed using a Student's t test, one-way ANOVA, or two-way ANOVA for experiments with two groups, three groups, or two different factors in more than two groups (genotype and mechanical ventilation), respectively. Nuclear mechanics measurements were compared using a repeated-measurements ANOVA. When appropriate, post hoc tests were

performed using the Tukey's HSD test. A two-sided *P* value lower than 0.05 was considered significant.

Sample sizes were estimated on the basis of preliminary results, with no formal calculations. In nonsignificant comparisons, statistical power to detect a difference of 0.75 points in histological score, a 20% in apoptotic rate, or a 75% change in gene expression was calculated. All the calculated power values were above 0.8 (table S2). Statistical analysis of genomic data was performed as described.

SUPPLEMENTARY MATERIALS

www.sciencetranslationalmedicine.org/cgi/content/full/10/456/eaam7598/DC1
Fig. S1. Changes in nuclear lamins with ventilation.
Fig. S2. Lamin-A and Lamin-B in airway epithelium and lung endothelium in patients.
Fig. S3. Changes in lamin content and nuclear compliance in epithelial cells and fibroblasts.
Fig. S4. Stretch-induced lung injury in Lamin-A–deficient mice ($Lmna^{LCS/LCS}$).
Fig. S5. Differences in the inflammatory response to ventilation between genotypes.
Fig. S6. Prelamin-A and Lamin-B abundance in $Zmpste24^{-/-}$ mice subjected to mechanical ventilation.
Fig. S7. Prelamin-A and Lamin-A staining after ventilation.
Fig. S8. Endotoxin-induced lung injury in wild-type and $Zmpste24^{-/-}$ mice.
Fig. S9. Principal components analysis of the microarray data.
Fig. S10. Differential mechanosensitive gene expression in wild-type and $Zmpste24^{-/-}$ mice subjected to mechanical ventilation.
Fig. S11. Differential expression of genes involved in apoptosis.
Fig. S12. Apoptosis after LPS injection in wild-type and $Zmpste24^{-/-}$ mice.
Fig. S13. Effects of HIV protease inhibitors in $Lmna^{LCS/LCS}$ mice.
Fig. S14. Effects of HIV protease inhibitors in $Zmpste24^{-/-}$ mice.
Fig. S15. Effects of lopinavir/ritonavir on the repair phase after VILI.
Fig. S16. Genetic and pharmacological blockade of the mechanical response to mechanical ventilation.
Fig. S17. Respiratory mechanics at baseline.
Table S1. Patients' characteristics.
Table S2. Statistical power of nonsignificant comparisons.
Table S3. Raw data.

REFERENCES AND NOTES

1. A. J. Engler, S. Sen, H. L. Sweeney, D. E. Discher, Matrix elasticity directs stem cell lineage specification. *Cell* **126**, 677–689 (2006).
2. N. Wang, J. D. Tytell, D. E. Ingber, Mechanotransduction at a distance: Mechanically coupling the extracellular matrix with the nucleus. *Nat. Rev. Mol. Cell Biol.* **10**, 75–82 (2009).
3. J. Swift, I. L. Ivanovska, A. Buxboim, T. Harada, P. C. Dingal, J. Pinter, J. D. Pajerowski, K. R. Spinler, J.-W. Shin, M. Tewari, F. Rehfeldt, D. W. Speicher, D. E. Discher, Nuclear lamin-A scales with tissue stiffness and enhances matrix-directed differentiation. *Science* **341**, 1240104 (2013).
4. J. C. Harr, T. R. Luperchio, X. Wong, E. Cohen, S. J. Wheelan, K. L. Reddy, Directed targeting of chromatin to the nuclear lamina is mediated by chromatin state and A-type lamins. *J. Cell Biol.* **208**, 33–52 (2015).
5. L. G. Fong, J. K. Ng, J. Lammerding, T. A. Vickers, M. Meta, N. Coté, B. Gavino, X. Qiao, S. Y. Chang, S. R. Young, S. H. Yang, C. L. Stewart, R. T. Lee, C. F. Bennett, M. O. Bergo, S. G. Young, Prelamin A and lamin A appear to be dispensable in the nuclear lamina. *J. Clin. Invest.* **116**, 743–752 (2006).
6. A. Tabuchi, H. T. Nickles, M. Kim, J. W. Semple, E. Koch, L. Brochard, A. S. Slutsky, A. R. Pries, W. M. Kuebler, Acute lung injury causes asynchronous alveolar ventilation that can be corrected by individual sighs. *Am. J. Respir. Crit. Care Med.* **193**, 396–406 (2016).
7. A. S. Slutsky, V. M. Ranieri, Ventilator-induced lung injury. *N. Engl. J. Med.* **369**, 2126–2136 (2013).
8. I. B. Copland, B. P. Kavanagh, D. Engelberts, C. McKerlie, J. Belik, M. Post, Early changes in lung gene expression due to high tidal volume. *Am. J. Respir. Crit. Care Med.* **168**, 1051–1059 (2003).
9. Acute Respiratory Distress Syndrome Network, R. G. Brower, M. A. Matthay, A. Morris, D. Schoenfeld, B. T. Thompson, A. Wheeler, Ventilation with lower tidal volumes as compared with traditional tidal volumes for acute lung injury and the acute respiratory distress syndrome. *N. Engl. J. Med.* **342**, 1301–1308 (2000).
10. E. Futier, J.-M. Constantin, C. Paugam-Burtz, J. Pascal, M. Eurin, A. Neuschwander, E. Marret, M. Beaussier, C. Gutton, J. Y. Lefrant, B. Allaouchiche, D. Verzilli, M. Leone, A. De Jong, J. E. Bazin, B. Pereira, S. Jaber; IMPROVE Study Group, A trial of intraoperative low-tidal-volume ventilation in abdominal surgery. *N. Engl. J. Med.* **369**, 428–437 (2013).
11. A. M. Pendás, Z. Zhou, J. Cadiñanos, J. M. P. Freije, J. Wang, K. Hultenby, A. Astudillo, A. Wernerson, F. Rodríguez, K. Tryggvason, C. López-Otín, Defective prelamin A processing and muscular and adipocyte alterations in Zmpste24 metalloproteinase–deficient mice. *Nat. Genet.* **31**, 94–99 (2002).
12. I. Varela, J. Cadiñanos, A. M. Pendás, A. Gutiérrez-Fernández, A. R. Folgueras, L. M. Sánchez, Z. Zhou, F. J. Rodríguez, C. L. Stewart, J. A. Vega, K. Tryggvason, J. M. P. Freije, C. López-Otín, Accelerated ageing in mice deficient in Zmpste24 protease is linked to p53 signalling activation. *Nature* **437**, 564–568 (2005).
13. C. Bougault, E. Aubert-Foucher, A. Paumier, E. Perrier-Groult, L. Huot, D. Hot, M. Duterque-Coquillaud, F. Mallein-Gerin, Dynamic compression of chondrocyte-agarose constructs reveals new candidate mechanosensitive genes. *PLOS ONE* **7**, e36964 (2012).
14. G. P. Sorescu, M. Sykes, D. Weiss, M. O. Platt, A. Saha, J. Hwang, N. Boyd, Y. C. Boo, J. D. Vega, W. R. Taylor, H. Jo, Bone morphogenic protein 4 produced in endothelial cells by oscillatory shear stress stimulates an inflammatory response. *J. Biol. Chem.* **278**, 31128–31135 (2003).
15. K. Grote, U. Bavendiek, C. Grothusen, I. Flach, D. Hilfiker-Kleiner, H. Drexler, B. Schieffer, Stretch-inducible expression of the angiogenic factor CCN1 in vascular smooth muscle cells is mediated by Egr-1. *J. Biol. Chem.* **279**, 55675–55681 (2004).
16. A.-R. Yoon, I. Stasinopoulos, J. H. Kim, H. M. Yong, O. Kilic, D. Wirtz, Z. M. Bhujwalla, S. S. An, COX-2 dependent regulation of mechanotransduction in human breast cancer cells. *Cancer Biol. Ther.* **16**, 430–437 (2015).
17. P. C. Schulze, G. W. de Keulenaer, K. A. Kassik, T. Takahashi, Z. Chen, D. I. Simon, R. T. Lee, Biomechanically induced gene *iex-1* inhibits vascular smooth muscle cell proliferation and neointima formation. *Circ. Res.* **93**, 1210–1217 (2003).
18. N. E. Hurley, L. A. Schildmeyer, K. A. Bosworth, Y. Sakurai, S. G. Eskin, L. H. Hurley, L. V. McIntire, Modulating the functional contributions of c-Myc to the human endothelial cell cyclic strain response. *J. Vasc. Res.* **47**, 80–90 (2010).
19. H. Zhou, Y. Li, G. Huang, X. Gu, J. Zeng, Y. Li, C. Luo, B. Ou, Y. Zhang, Z. Wu, L. Tang, Interleukin 6 augments mechanical strain-induced C-reactive protein synthesis via the stretch-activated channel–nuclear factor κ B signal pathway. *Heart* **99**, 570–576 (2013).
20. J. Dunn, S. Thabet, H. Jo, Flow-dependent epigenetic DNA methylation in endothelial gene expression and atherosclerosis. *Arterioscler. Thromb. Vasc. Biol.* **35**, 1562–1569 (2015).
21. Y. Imai, J. Parodo, O. Kajikawa, M. de Perrot, S. Fischer, V. Edwards, E. Cutz, M. Liu, S. Keshavjee, T. R. Martin, J. C. Marshall, V. M. Ranieri, A. S. Slutsky, Injurious mechanical ventilation and end-organ epithelial cell apoptosis and organ dysfunction in an experimental model of acute respiratory distress syndrome. *JAMA* **289**, 2104–2112 (2003).
22. C. Coffinier, S. E. Hudon, E. A. Farber, S. Y. Chang, C. A. Hrycyna, S. G. Young, L. G. Fong, HIV protease inhibitors block the zinc metalloproteinase ZMPSTE24 and lead to an accumulation of prelamin A in cells. *Proc. Natl. Acad. Sci. U.S.A.* **104**, 13432–13437 (2007).
23. H. Q. Le, S. Ghatak, C.-Y. C. Yeung, F. Tellkamp, C. Günschmann, C. Dieterich, A. Yeroslaviz, B. Habermann, A. Pombo, C. M. Niessen, S. A. Wickström, Mechanical regulation of transcription controls Polycomb-mediated gene silencing during lineage commitment. *Nat. Cell Biol.* **18**, 864–875 (2016).
24. A. Schwingshackl, The role of stretch-activated ion channels in acute respiratory distress syndrome: Finally a new target? *Am. J. Physiol. Lung Cell. Mol. Physiol.* **311**, L639–L652 (2016).
25. G. Gawlak, Y. Tian, J. J. O'Donnell III, X. Tian, A. A. Birukova, K. G. Birukov, Paxillin mediates stretch-induced Rho signaling and endothelial permeability *via* assembly of paxillin-p42/44MAPK-GEF-H1 complex. *FASEB J.* **28**, 3249–3260 (2014).
26. J. Lammerding, P. C. Schulze, T. Takahashi, S. Kozlov, T. Sullivan, R. D. Kamm, C. L. Stewart, R. T. Lee, Lamin A/C deficiency causes defective nuclear mechanics and mechanotransduction. *J. Clin. Invest.* **113**, 370–378 (2004).
27. A. Buxboim, J. Swift, J. Irianto, K. R. Spinler, P. C. Dingal, A. Athirasala, Y. R. Kao, S. Cho, T. Harada, J. W. Shin, D. E. Discher, Matrix elasticity regulates lamin-A, C phosphorylation and turnover with feedback to actomyosin. *Curr. Biol.* **24**, 1909–1917 (2014).
28. I. L. Ivanovska, J. W. Shin, J. Swift, D. E. Discher, Stem cell mechanobiology: Diverse lessons from bone marrow. *Trends Cell Biol.* **25**, 523–532 (2015).
29. G. Matute-Bello, J. S. Lee, W. C. Liles, C. W. Frevert, S. Mongovin, V. Wong, K. Ballman, S. Sutlief, T. R. Martin, Fas-mediated acute lung injury requires Fas expression on nonmyeloid cells of the lung. *J. Immunol.* **175**, 4069–4075 (2005).
30. C. G. Lee, S. J. Cho, M. J. Kang, S. P. Chapoval, P. J. Lee, P. W. Noble, T. Yehualaeshet, B. Lu, R. A. Flavell, J. Milbrandt, R. J. Homer, J. A. Elias, Early growth response gene 1–mediated apoptosis is essential for transforming growth factor β_1–induced pulmonary fibrosis. *J. Exp. Med.* **200**, 377–389 (2004).
31. A. Vadivel, S. Abozaid, T. van Haaften, M. Sawicka, F. Eaton, M. Chen, B. Thebaud, Adrenomedullin promotes lung angiogenesis, alveolar development, and repair. *Am. J. Respir. Cell Mol. Biol.* **43**, 152–160 (2010).

32. S. K. Kolluri, N. Bruey-Sedano, X. Cao, B. Lin, F. Lin, Y.-H. Han, M. I. Dawson, X.-k. Zhang, Mitogenic effect of orphan receptor TR3 and its regulation by MEKK1 in lung cancer cells. *Mol. Cell. Biol.* **23**, 8651–8667 (2003).
33. M. de Vries, I. H. Heijink, R. Gras, L. E. den Boef, M. Reinders-Luinge, S. D. Pouwels, M. N. Hylkema, M. van der Toorn, U. Brouwer, A. J. M. van Oosterhout, M. C. Nawijn, Pim1 kinase protects airway epithelial cells from cigarette smoke-induced damage and airway inflammation. *Am. J. Physiol. Lung Cell. Mol. Physiol.* **307**, L240–L251 (2014).
34. R. Blundell, D. J. Harrison, S. O'Dea, p21(Waf1/Cip1) regulates proliferation and apoptosis in airway epithelial cells and alternative forms have altered binding activities. *Exp. Lung Res.* **30**, 447–464 (2004).
35. M. L. Wynn, A. C. Ventura, J. A. Sepulchre, H. J. García, S. D. Merajver, Kinase inhibitors can produce off-target effects and activate linked pathways by retroactivity. *BMC Syst. Biol.* **5**, 156 (2011).
36. A. González-López, A. Astudillo, E. Garcia-Prieto, M. S. Fernández-García, A. López-Vázquez, E. Batalla-Solis, F. Taboada, A. Fueyo, G. M. Albaiceta, Inflammation and matrix remodeling during repair of ventilator-induced lung injury. *Am. J. Physiol. Lung Cell. Mol. Physiol.* **301**, L500–L509 (2011).
37. S. Perrin, J. Cremer, O. Faucher, J. Reynes, P. Dellamonica, J. Micallef, C. Solas, B. Lacarelle, C. Stretti, E. Kaspi, A. Robaglia-Schlupp, C. Nicolino-Brunet, C. Tamalet, N. Levy, I. Poizot-Martin, P. Cau, P. Roll, HIV protease inhibitors do not cause the accumulation of prelamin A in PBMCs from patients receiving first line therapy: The ANRS EP45 "aging" study. *PLOS ONE* **7**, e53035 (2012).
38. A. D. Badley, In vitro and in vivo effects of HIV protease inhibitors on apoptosis. *Cell Death Differ.* **12** (suppl. 1), 924–931 (2005).
39. J.-W. Shin, K. R. Spinler, J. Swift, J. A. Chasis, N. Mohandas, D. E. Discher, Lamins regulate cell trafficking and lineage maturation of adult human hematopoietic cells. *Proc. Natl. Acad. Sci. U.S.A.* **110**, 18892–18897 (2013).
40. G. Matute-Bello, G. Downey, B. B. Moore, S. D. Groshong, M. A. Matthay, A. S. Slutsky, W. M. Kuebler; Acute Lung Injury in Animals Study Group, An official American Thoracic Society workshop report: Features and measurements of experimental acute lung injury in animals. *Am. J. Respir. Cell Mol. Biol.* **44**, 725–738 (2011).
41. C. Kilkenny, W. J. Browne, I. C. Cuthill, M. Emerson, D. G. Altman, Improving bioscience research reporting: The ARRIVE guidelines for reporting animal research. *PLOS Biol.* **8**, e1000412 (2010).
42. I. López-Alonso, A. Aguirre, A. González-López, Á. F. Fernandez, L. Amado-Rodríguez, A. Astudillo, E. Batalla-Solis, G. M. Albaiceta, Impairment of autophagy decreases ventilator-induced lung injury by blockade of the NF-κB pathway. *Am. J. Physiol. Lung Cell. Mol. Physiol.* **304**, L844–L852 (2013).
43. J. Blázquez-Prieto, I. López-Alonso, L. Amado-Rodríguez, E. Batalla-Solís, A. González-López, G. M. Albaiceta, Exposure to mechanical ventilation promotes tolerance to ventilator-induced lung injury by *Ccl3* downregulation. *Am. J. Physiol. Lung Cell. Mol. Physiol.* **309**, L847–L856 (2015).
44. ARDS Definition Task Force, V. M. Ranieri, G. D. Rubenfeld, B. T. Thompson, N. D. Ferguson, E. Caldwell, E. Fan, L. Camporota, A. S. Slutsky, Acute respiratory distress syndrome: The Berlin Definition. *JAMA* **307**, 2526–2533 (2012).
45. I. Ivanovska, J. Swift, T. Harada, J. D. Pajerowski, D. E. Discher, Physical plasticity of the nucleus and its manipulation. *Methods Cell Biol.* **98**, 207–220 (2010).

Acknowledgments: We thank C. López-Otin, F. G. Osorio, A. Fueyo, C. Bárcena, and L. del Campo for the gift of mutant mice and their invaluable help during the development of this work, D. Navajas for his comments on nuclear mechanics studies, and M. Pitiot for her collaboration with histological studies. **Funding:** Supported by Instituto de Salud Carlos III (Plan Estatal I+D+i, PI13/02189 and PI16/01614, FEDER funds). I.L.-A. is the recipient of grants from Fundación para el fomento en Asturias de la investigación científica aplicada y la tecnología (FICYT; GRUPIN14-089, Consejería de Hacienda, Principado de Asturias, Spain) and Fundación Asturcor. C.H. is the recipient of a grant from Instituto de Salud Carlos III (Contratos Sara Borrell, CD16/00033). L.A.-R. is the recipient of a grant from Instituto de Salud Carlos III (Contratos Rio Hortega, CM16/00128). G.M.A. is the recipient of a grant from Instituto de Salud Carlos III (INT-15/002). Instituto Universitario de Oncología is supported by Fundación Bancaria Caja de Ahorros de Asturias. **Author contributions:** G.M.A. was responsible for the study concept and holds the responsibility for the data integrity. I.L.-A., A.G.-L., and G.M.A. designed the experiments. I.L.-A., J.B.-P., L.A.-R., and A.G.-L. performed the animal experiments, obtained the samples, and made the in vivo measurements. I.L.-A., J.B.-P., C.H., and C.L.-M. performed the biochemical analyses, including Western blotting qPCR and sample processing for microarray experiments. L.A.-R. collected patients' data. I.L.-A., G.M.A., and A.G.-L. performed the cell culture studies. A.A. contributed to the histological and electron microscopy studies. I.L.-A. and M.S. performed the measurements of nuclear compliance. G.M.A. and I.L.-A. analyzed the data. G.M.A. and C.C.d.S. were responsible for the analyses of genomic data. G.M.A., I.L.-A., and C.C.d.S. wrote the manuscript. All authors reviewed the final version. **Competing interests:** The authors declare that they have no competing interests. **Data and materials availability:** Genomic data have been deposited in GEO (accession number GSE85269). The rest of the data associated with this study are present in the paper or the Supplementary Materials.

Submitted 16 January 2017
Resubmitted 30 August 2017
Accepted 25 January 2018
Published 29 August 2018
10.1126/scitranslmed.aam7598

Citation: I. López-Alonso, J. Blázquez-Prieto, L. Amado-Rodríguez, A. González-López, A. Astudillo, M. Sánchez, C. Huidobro, C. López-Martínez, C. C. dos Santos, G. M. Albaiceta, Preventing loss of mechanosensation by the nuclear membranes of alveolar cells reduces lung injury in mice during mechanical ventilation. *Sci. Transl. Med.* **10**, eaam7598 (2018).

Science Translational Medicine

Preventing loss of mechanosensation by the nuclear membranes of alveolar cells reduces lung injury in mice during mechanical ventilation

Inés López-Alonso, Jorge Blázquez-Prieto, Laura Amado-Rodríguez, Adrián González-López, Aurora Astudillo, Manuel Sánchez, Covadonga Huidobro, Cecilia López-Martínez, Claudia C. dos Santos and Guillermo M. Albaiceta

Sci Transl Med **10**, eaam7598.
DOI: 10.1126/scitranslmed.aam7598

Softening the effects of lung ventilation

Mechanical ventilation is a life support treatment that helps patients to breathe; however, the mechanical stress caused by artificial pressure can cause lung injury. The molecular mechanisms responsible for this adverse event are not completely understood. Now, López-Alonso *et al*. show that Lamin-A overexpression induced by mechanical ventilation increased nuclear membrane stiffness (that is, reduced compliance) in lung alveolar cells and contributed to lung injury in mice. Inhibition of nuclear Lamin-A production using two protease inhibitors approved for treating human immunodeficiency virus infection preserved alveolar nuclear membrane compliance and reduced lung injury induced by mechanical ventilation. The results suggest that protease inhibitors might be useful for reducing the side effects associated with mechanical ventilation.